

PCCP

Accepted Manuscript



This article can be cited before page numbers have been issued, to do this please use: H. Jung, B. C. Yeo, K. Lee and S. S. Han, *Phys. Chem. Chem. Phys.*, 2016, DOI: 10.1039/C6CP06158C.



This is an Accepted Manuscript, which has been through the Royal Society of Chemistry peer review process and has been accepted for publication.

Accepted Manuscripts are published online shortly after acceptance, before technical editing, formatting and proof reading. Using this free service, authors can make their results available to the community, in citable form, before we publish the edited article. We will replace this Accepted Manuscript with the edited and formatted Advance Article as soon as it is available.

You can find more information about Accepted Manuscripts in the [Information for Authors](#).

Please note that technical editing may introduce minor changes to the text and/or graphics, which may alter content. The journal's standard [Terms & Conditions](#) and the [Ethical guidelines](#) still apply. In no event shall the Royal Society of Chemistry be held responsible for any errors or omissions in this Accepted Manuscript or any consequences arising from the use of any information it contains.

Atomistics of the Lithiation of Oxidized Silicon (SiO_x) Nanowires in Reactive Molecular Dynamics Simulations

Hyun Jung,^{†,‡} Byung Chul Yeo,[†] Kwang-Ryeol Lee,[†] and Sang Soo Han^{†,}*

[†]Center for Computational Science, Korea Institute of Science and Technology (KIST),
Hwarangno 14-gil 5, Seongbuk-gu, Seoul 136-791, Republic of Korea

[‡]Department of Physics, Hanyang University, 222 Wangsimni-ro, Seongdong-gu, Seoul 133-
791, Republic of Korea

Corresponding Author

*sangsoo@kist.re.kr. Tel.: +82 2 958 5441. Fax: +82 2 958 5451.

ABSTRACT

Although silicon oxide (SiO_x) nanowires (NWs) are recognized as a promising anode material for lithium-ion batteries (LIBs), a clear understanding of their lithiation mechanism has not yet been reported. We elucidate the lithiation mechanism of SiO_x NWs at the atomic scale based on molecular dynamics (MD) simulations employing the ReaxFF reactive force field developed through first-principles calculations. SiO_x NWs with crystalline Si (*c*-Si) core and amorphous SiO_2 (*a*- SiO_2) shell structures of ~ 1 nm in thickness show smaller volume expansion than do pristine Si NWs, as found in previous experiments. Lithiation into SiO_x NWs creates two interfaces: *c*-Si/*a*- Li_xSi and *a*- $\text{Li}_x\text{Si}/a- Li_ySiO_2 . The mobility of the latter, which is located farther toward the outside of the NW, is slower than that of the former, which is one of the reasons why the thin SiO_2 layer can suppress the volume expansion of SiO_x NWs during lithiation. Another reason can be found from the stress distribution, as the SiO_x NWs have a different stress distribution from the pristine case. Moreover, the lithiation of SiO_x NWs leads to the formation of Li_2O and Li_4SiO_4 compounds in the oxide layer, where several Li atoms (not a majority) in the Li_4SiO_4 can escape from the compound and diffuse into the *c*-Si, in contrast to the Li_2O case. However, Li atoms that pass through the SiO_2 layer penetrate into the *c*-Si preferentially along the $<110>$ or $<112>$ direction, similar to the mechanism observed in pristine Si NWs. We expect that our comprehensive understanding of the lithiation mechanism of SiO_x NWs will provide helpful guidance for the design of SiO_x anodes to obtain better performing LIBs.$

1. Introduction

As a promising anode material for lithium (Li)-ion batteries (LIB), silicon (Si) has received much interest because it has a much higher specific capacity than graphite, which is widely used in current LIBs.¹⁻⁴ However, it also exhibits significant volume fluctuations during the insertion/extraction of Li ions, which leads to fracturing of the material followed by rapid capacity fading owing to the loss of electrical continuity.^{1,5,6}

To overcome this disadvantage of Si, several approaches have been considered thus far. In particular, nano-sized pillar structures such as nanowires and nanotubes can markedly reduce the fracturing of Si during cycles of the insertion/extraction of Li ions.⁷⁻¹³ A conductive coating such as carbon is also a promising possibility because it can increase electrical continuity.¹⁴⁻¹⁵ For example, encapsulation in crumpled graphene shells has been found to greatly improve several aspects of the performance of Si, such as Coulombic efficiency, cycling stability, and rate capability.¹⁶

Silicon suboxides, SiO_x ($x < 2$), have also been considered as potential LIB anodes.¹⁷⁻²² It has been suggested that SiO_x may form Si nanocrystallites dispersed in an amorphous SiO_2 ($a\text{-SiO}_2$) matrix.²³⁻²⁷ Surface passivation using SiO_2 improves the cyclic properties of Si anodes. Indeed, Si anodes coated with native SiO_x layers can withstand more than 6,000 cycles with little capacity fading.²⁸ Surface passivation can effectively alleviate the stress and manage the deformation of Si anodes that are induced during Li insertion/extraction.²⁹⁻³⁰ Moreover, it can prevent the continual shedding and reforming of the solid electrolyte interface (SEI), thus having a beneficial effect on battery performance.³¹⁻³³ SiO_2 shows a reversible Li capacity of up to 2/3Li per Si,³⁴ although it is typically thought that metal oxides act as insulators for electrons and usually have low ion permittivity.³⁵ Moreover, in situ transmission electron

microscopy shows that lithiation into a sub-10 nm SiO₂ thin film leads to a volumetric strain of ~200 %.³⁶ Metal oxides are typically brittle, meaning that they fracture at a small deformation upon loading. Thus, the question of how the SiO₂ thin layer can sustain such a large deformation during lithiation is very intriguing.

Based on a first-principles calculation, the lithiation behaviors of silicon-rich oxides (e.g., SiO_{1/3}) have been reported.³⁷ In this case, the silicon oxide was considered as a homogenous phase, rather than a composite phase such as Si nanocrystallites dispersed in *a*-SiO₂. Similarly, the lithiation of a hydroxylated surface of *a*-SiO₂ have been investigated.³⁸ However, the atomistic understanding of the lithiation behaviors of composite-phase SiO_x materials is still limited.

In this work, we report the atomistic lithiation behaviors of SiO_x nanowires (NWs) with composite structures of the *c*-Si/*a*-SiO₂ core/shell type based on molecular dynamics (MD) simulation employing the ReaxFF reactive force field at the atomic level. We present the structural evolution of SiO_x NWs during lithiation and clarify how the SiO₂ surface film can reduce the volume expansion of a Si anode during lithiation.

2. Computational details

To simulate the lithiation behavior of SiO_x NWs at the atomic level, we used an MD simulation employing the ReaxFF^{39,40} which can describe chemical reactions between atoms (e.g., bond formation/breaking). Recently, we successfully clarified the lithiation behavior of a pristine Si NW by means of such a ReaxFF-MD simulation, in which the ReaxFF parameters for the Li-Si system were developed through first-principles calculations.⁴¹ Because the ReaxFF for the Li-Si-O ternary system is required to investigate the lithiation of

SiO_x , we extended the previous Li-Si ReaxFF and developed additional ReaxFF parameters (e.g., Li-O bond parameters) in this work. These additional parameters were developed based on data calculated from first-principles. The ReaxFF was optimized using a successive one-parameter search technique.^{42,43} Details regarding the development of the ReaxFF are explained in the electronic supplementary information (ESI).

The MD simulations were performed using the LAMMPS⁴⁴ software on the iBat simulation platform (<http://battery.vfab.org>) for LIBs, which was recently developed by our research group. To integrate Newton's equations of motion during the MD simulations, a Verlet⁴⁵ algorithm was used with a time step of 0.5 femtoseconds (fs). All calculations were performed in a canonical NVT ensemble at 300 K, in which the temperature was maintained by a Nosé-Hoover thermostat⁴⁶ with a damping parameter of 0.01 fs⁻¹.

Prior to the simulation of the lithiation of SiO_x NWs, we obtained the NWs through chemical reactions between O_2 molecules and pristine Si NWs (~5 nm in diameter and ~10 nm in length), which were also simulated by the ReaxFF-MD simulations. Three SiO_x NWs with different oxide thicknesses (i.e. 4, 8, and 10 Å) were considered, where the composition of each NW corresponded to $\text{SiO}_{0.14}$, $\text{SiO}_{0.29}$, and $\text{SiO}_{0.32}$, respectively. The detailed procedure for obtaining the SiO_x NWs can be found in Figure S5 of the ESI. By analyzing the concentrations of atoms in the obtained SiO_x NWs, it was found that the compositions of the silicon oxides in the three SiO_x types corresponded to SiO_2 . In other words, the three NWs obtained in the ReaxFF-MD simulations had the Si/ SiO_2 core/shell structures.

For the simulation of the lithiation of the SiO_x NWs, a method similar to that used in our previous work⁴¹ to investigate the lithiation of pristine Si NWs was applied. The SiO_x NWs (Si/ SiO_2 core/shell structures) were immersed in a simulation cell with dimensions of 105.2 Å

$\times 105.2 \text{ \AA} \times 97.8 \text{ \AA}$ that was filled with Li atoms, and any Li atoms that overlapped the SiO_x NWs were removed. The total number of atoms in the system was approximately 100,000. Additionally, periodic boundary conditions in the x , y , and z directions were applied during the MD simulations, in which the NW axis lays in the z direction, leading to lithiation of the SiO_x NWs along the x and y directions.

3. Results and discussion

The lithiation behaviors of the SiO_x NWs that were obtained from the ReaxFF-MD simulations are shown in Figure 1, in which the behavior of a pristine Si NW is also presented for comparison. The pristine Si NW shows a volume expansion of 278 %, with a concentration of $\text{Li}_{3.64}\text{Si}$ after 2,000 pico seconds (ps) of lithiation. By contrast, the SiO_x NWs show smaller volume expansions than that of pristine Si NW. For example, the $\text{Si}_{0.14}$ and $\text{SiO}_{0.29}$ NWs show volume expansion of 281 % and 229 % after 2,000 ps of lithiation, respectively, although they have higher Li concentrations ($\text{Li}_{4.48}\text{SiO}_{0.14}$ and $\text{Li}_{3.93}\text{SiO}_{0.29}$) than $\text{Li}_{3.64}\text{Si}$ in the pristine case.

We additionally analyzed the volume expansion and Li capacity of the SiO_x NWs as functions of MD time and obtained the relationships for volume expansion versus Li capacity, which are shown in Figure 2. The SiO_x NWs show similar trends of volume expansion versus Li capacity, regardless of their surface oxide (SiO_2) thickness. It is also apparent that the SiO_x NWs exhibit smaller volume expansions than that of the pristine Si NW at a given Li capacity. Indeed, a previous experiment²⁹ has indicated that for Si NWs with native SiO_2 the surface oxide suppresses the volume expansion during lithiation, which is well consistent with our simulation.

To investigate the structural evolution of SiO_x NWs during lithiation, we analyzed the radial distribution functions (RDFs) for Si-Si, Si-O, Si-Li, and Li-O pairs (Figure 3), where the RDF is defined as the number of neighbors of a given species per unit volume as a function of distance. For the Si-Si pair, the initial structure of the pristine Si NW (0 ps) shows sharp peaks at 2.4, 3.9, and 4.6 Å, which correspond to the first, second, and third nearest-neighbor distances, respectively, between two Si atoms in the crystalline Si (*c*-Si) phase. Likewise, the initial structures of the SiO_x NWs also show such sharp peaks, although the peak intensities are lower than those for the pristine Si NW. The peak intensities for the SiO_x NWs decrease with increasing thickness of the surface oxide. These findings indicate that the initial structures of the SiO_x NWs still contain crystalline Si phases, although a surface oxide (SiO_2) has formed. Of course, the crystallinity decreases with increasing oxide thickness. During lithiation, the first nearest-neighbor peak for the Si-Si pair in all NWs (pristine Si and SiO_x) shifts to 2.9 Å from the original 2.4 Å, accompanied by a decrease in the peak intensity. For not only the pristine Si NW but also the SiO_x NWs, lithiation leads to amorphization of the NWs, induced by the increase in the Si-Si bond distance and subsequent bond breaking.

For the Si-O pair, lithiation causes the intensity of the first nearest-neighbor peak to decrease, but the peak position (1.7 Å) remains nearly unchanged. By contrast, the peak intensities of Si-Li and O-Li pairs increase during lithiation, indicating increased interaction of Li atoms with Si and O atoms.

According to the coordination numbers (CNs) (Figure S6) calculated by integrating the first peak in the RDF in Figure 3, $\text{CN}_{\text{Si-Si}}$ and $\text{CN}_{\text{Si-O}}$ drop from 4.0 and 2.2 to 2.2 and 0.9, respectively, as MD time increases (as lithiation proceeds). This is because of the disintegration of the SiO_x NWs during lithiation. These low-connectivity Si and isolated O

atoms are surrounded by Li atoms, as evidenced by increases in CN_{Si-Li} and CN_{O-Li}. For example, CN_{Si-Li} gradually increases from 3.0 at 250 ps to 6.0 at 2,000 ps, while CN_{O-Li} increases to 2.0 at 2,000 ps.

The lithiation of a pristine crystalline Si NW creates an interface between a *c*-Si phase and an *a*-Li_xSi phase.⁴¹ Likewise, the lithiation of SiO_x NWs with a core/shell structure of *c*-Si and *a*-SiO₂ leads to the formation of two interfaces, an *a*-Li_ySiO₂/*a*-Li_xSi interface and an *a*-Li_xSi/*c*-Si interface, which are presented in Figure 4 as blue and green interfaces, respectively, whereas the initial structure of the SiO_x NWs contain an interface between the *c*-Si core and the *a*-SiO₂ shell. To investigate the movement of the interfaces (blue and green interfaces) in SiO_x NWs that are generated during lithiation, we detected the positions of these interfaces as functions of MD time. From a comparison of the interface positions at 1,000 and 2,000 ps, it is clear that the Li_ySiO₂/*a*-Li_xSi interface is more strongly anchored than the *a*-Li_xSi/*c*-Si interface during lithiation, where the former is located nearer the NW surface than the latter. In other words, the mobility of the interface between the *c*-Si and *a*-Li_xSi phases is 2.5 times higher than that of the interface between the Li_ySiO₂ and *a*-Li_xSi phases, which is shown in Figure S7.

While further investigating the Li_ySiO₂ phase, we observed the formation of Li₂O and Li₄SiO₄ compounds (Figure 5), which has also been found in several experiments³⁶ and theories⁴⁷. Most Li₄SiO₄ compounds reach saturation within 200 ps, whereas the formation of Li₂O gradually increases up through 1,000 ps and then saturates. According to our simulation, the numbers of Li₂O compounds are much higher than those of Li₄SiO₄. At 2,000 ps, Li₂O compounds are approximately 25 times more abundant than Li₄SiO₄ compounds. The diffusivities of such Li₂O and Li₄SiO₄ compounds are lower than that of Li “atoms”. Thus,

the formation of these Li_2O and Li_4SiO_4 compounds can hinder the movement of the $\text{Li}_x\text{SiO}_2/a\text{-Li}_x\text{Si}$ interface, as seen in Figure 4.

A previous experiment has also reported the formation of Li_2SiO_5 after the lithiation of a SiO_2 thin film,⁴⁸ although this was not observed in our simulation. However, in an experiment³⁶ on the lithiation of a sub-10 nm SiO_2 thin film similar to our case, the presence of Li_2SiO_5 was not observed, although Li_2O and Li_4SiO_4 were found, which supports our simulation results.

To further explore the constraining effect of the SiO_2 layer, we calculated the residual stress distributions of the SiO_x NWs with *c*-Si/*a*- SiO_2 core/shell structures in the radial direction (σ_r) and then compared the results with those for the pristine Si NW, as shown in Figure 6. The residual stress was obtained by averaging the atomic stresses of all atoms in the concentric shell between r and $r + \delta r$, where r is the radial distance from the center of the NW. The radial stress (σ_r) is calculated with the Eq (1).⁴⁹

$$\sigma_r = \sigma_{xx} \cos^2 \theta + 2\sigma_{xy} \sin \theta \cos \theta + \sigma_{yy} \sin^2 \theta \quad (1)$$

where the σ_{xx} and σ_{xy} are the normal and shear stresses in a x-y-z coordinate system, respectively, and the θ is an angle.

As explained in Figure 4, the lithiation of a pristine *c*-Si NW creates an interface between the *c*-Si and *a*- Li_xSi phases. This interface has compressive (negative) stresses and plays the role of a stress buffer between the *c*-Si and *a*- Li_xSi phases, as seen in Figure 6a. In other words, the *a*- Li_xSi phase has tensile (positive) stresses, which serve as a driving force for the volume

expansion of the NW.

In the initial SiO_x NWs (0 ps), the *c*-Si core is subject to compressive stresses that are induced by the tensile stresses of the *a*- SiO_2 shell. As discussed in Figure 4, the lithiation of a SiO_x NW with a core/shell structure of *c*-Si and *a*- SiO_2 leads to the formation of two interfaces, a *c*-Si/*a*- Li_xSi interface (interface I) and an *a*- Li_xSi /*a*- Li_ySiO_2 interface (interface II). These interfaces also act as buffer layers alleviating abrupt changes in stresses. Here, the *a*- Li_ySiO_2 phase possesses tensile stresses, which lead to stress distributions in the *a*- Li_xSi phase and at the interface I that are different from those observed in the pristine Si NW case. In a SiO_x NW, both the *a*- Li_xSi phase and interface II are subject to compressive stresses, unlike the pristine Si NW case, in which the *a*- Li_xSi phase has tensile stresses. Such compressive stresses exerted on the *a*- Li_xSi phase induce a retardation effect on the volume expansion of the NW during lithiation. The *a*- SiO_2 has a stronger stiffness (37 GPa)⁵⁰ than highly lithiated Li_xSi (e.g., $\text{Li}_{15}\text{Si}_4$ = 28 GPa),⁵¹ where a stronger stiffness indicates that a higher energy is required for the constant volume change. Due to the stronger stiffness of the SiO_2 layer, the SiO_x NWs shows significantly different stress distributions in comparison to the pristine Si NWs.

The tensile stress is a driving force for the volume expansion of the Si and SiO_x NWs. And a distribution of the tensile stress exerted in a shell region of the NWs can be an indicator to evaluate a degree of the volume expansion. In Figure 6, the pristine Si NW after lithiation of 500 ps has the tensile stress distribution of 45 Å, which is wider than that (15 Å) observed in the SiO_x NW. In addition, the volume expansion is also determined by the net of integrated tensile and compressive stresses. After lithiation of 500 ps, the pristine Si NW has the net value of 276.9×10^4 GPa·Å, while the SiO_x NW has the smaller value of 254.7×10^4 GPa·Å.

because of high compressive stresses exerted in the $a\text{-Li}_x\text{Si}$ phase and interface II.

The atomistic lithiation mechanism of oxidized Si NWs has not previously been clearly understood. Recently, we proposed a lithiation mechanism for pristine Si NWs.⁴¹ During the lithiation process, Li atoms penetrate into the lattices of *c*-Si NWs preferentially along the <110> or <112> direction, and the *c*-Si then transforms into the $a\text{-Li}_x\text{Si}$ phase as a result of the simultaneous breaking of Si-Si bonds; here, the formation of silicene-like structures in the NWs is observed before the full amorphization of the Si NWs.⁴¹ Likewise, this phenomenon is also observed in SiO_x NWs, as shown in Figure 7. However, in SiO_x NWs, the Li atoms first interact with the SiO_2 shell layer, and then, lithium oxides and lithium silicates such as Li_2O and Li_4SiO_4 are generated in the oxide layer. *Simultaneously*, Li atoms passing through the SiO_2 layer without formation of the Li_2O and Li_4SiO_4 can also diffuse into the *c*-Si phase, where they penetrate into the *c*-Si with a preference for the <110> or <112> direction, as confirmed by the formation of silicene-like structures (Figure 7*h* and *i*). Further lithiation leads to the disappearance of these silicene-like structures through Si-Si bond breaking. This process of penetration into the *c*-Si is similar to that observed in the case of pristine Si NWs. Moreover, the diffusion rate in the $a\text{-SiO}_2$ phase is slower than that in the *c*-Si phase, which can be supported by a previous DFT calculation.⁴⁷ Thus, the amount of *c*-Si in a SiO_x NW is larger than that in a pristine NW at a given MD time, as can be seen from a comparison of Figure 7*e* and *j*.

Interestingly, although most of the Li_4SiO_4 compounds are stable, we find several unstable Li_4SiO_4 compounds (not a majority) that show dissociation and recombination phenomena. Li atoms from Li_4SiO_4 can diffuse into the Si core region of a Si NW (dissociation behavior: $\text{Li}_4\text{SiO}_4 \rightarrow 4\text{Li}^+ + \text{SiO}_4^{4-}$); then, other Li atoms bind to the generated SiO_4^{4-} , and thus

Li_4SiO_4 quickly reforms (recombination behavior: $4\text{Li}^+ + \text{SiO}_4^{4-} \rightarrow \text{Li}_4\text{SiO}_4$). As shown in Figure 8, one Li atom in the Li_4SiO_4 compound formed at 500 ps can diffuse into the Si core of the NW at 1,000 ps; subsequently, all Li atoms in the original Li_4SiO_4 are substituted by others at 2,000 ps. No such dissociation and recombination processes are observed in the Li_2O compounds. The main reason for such behaviors is because of the difference of Li binding energies. According to our DFT calculation, a Li binding energy in the Li_2O compound is 108 kcal/mol, which is higher than 76 kcal/mol in the Li_4SiO_4 .

In this work, we focus on the lithiation process of SiO_x NWs; however, for the practical anode material of LIBs, the delithiation process should also be investigated. Using the ReaxFF-MD simulation, one can simulate the delithiation process, where a force $F = qE$ is added to each charged atom due to an external electric field being applied to the system. The relevant result is also found in Figure S8. The detail study on the cycleability of SiO_x NWs will be additionally reported in the near future.

4. Summary and conclusion

By means of MD simulations employing the ReaxFF, we elucidated the atomistic lithiation mechanism of SiO_x NWs with *c*-Si/*a*- SiO_2 core/shell structures. Li atoms interact with the *a*- SiO_2 layer, generating Li_2O and Li_4SiO_4 compounds. Subsequently, other Li atoms that do not bind to the *a*- SiO_2 layer diffuse into the *c*-Si core, where they penetrate the *c*-Si preferentially along the $<110>$ or $<112>$ direction. Interestingly, several Li atoms in Li_4SiO_4 compounds can also penetrate into the *c*-Si core, although not the majority. We find that an *a*- SiO_2 layer with a thickness of ~ 1 nm can indeed suppress the volume expansion of a SiO_x NW during the lithiation process, which is supported by several previous experiments.

During the lithiation of a SiO_x NW, two interfaces are created, one between the *c*-Si and *a*- Li_xSi phases (interface I) and one between the *a*- Li_xSi and *a*- Li_ySiO_2 phases (interface II), of which interface II is located farther toward the outside of the NW. The mobility of interface II, which involves silicon oxide layers, is slower than that of interface I. In addition, the *a*- SiO_2 shell layer induces different stress distributions in the SiO_x NW compared with those in pristine Si NW. In a pristine Si NW, the Li_xSi phase formed during the lithiation process is under tensile stresses, which lead to the observed volume expansion behavior. By contrast, the Li_xSi phase formed during the lithiation of a SiO_x NW is subject to compressive stresses, exerting a suppression effect on the volume expansion. Therefore, because of these differences in stress distribution, a SiO_x NW exhibits a smaller volume expansion than does a pristine Si NW. These findings strongly suggest that SiO_x NWs with thin SiO_2 layers are a promising anode material for Li-ion batteries.

Moreover, we expect that our comprehensive characterization of the lithiation mechanism of SiO_x NWs will provide beneficial insight to guide the future design of improved Si-based anodes. According to this work, a thin coating layer, which has a stiffness higher than the $\text{Li}_{15}\text{Si}_4$ (as a representative of highly lithiated Li_xSi phases), would provide such a volume suppression effect. Of course, Li atoms should be also able to pass through the coating layer. As an example of such a coating layer, Al_2O_3 (stiffness: 255 GPa)⁵² can be considered. Indeed, several studies^{43,53,54} shows beneficial effects of the Al_2O_3 coating layer on the battery performances.

In addition, using the ReaxFF-MD simulations, we have been currently studying effects of carbon coating (e.g., graphene and carbon nanotubes) on lithiation, delithiation, and cycleability of SiO_x , and designing an optimum SiO_x anode material with homogeneous

Published on 25 October 2016. Downloaded by Vanderbilt University Library on 25/10/2016 15:22:22.

phases which is different from a core-shell structure in this work. In particular, according to a recent finding,⁵⁵ deformation ability and strength of the SiNWs are remarkably improved after the carbon nanotube encapsulation. Also, we have been exploring formation of solid-electrolyte interfaces on Si-based anodes for LIBs has been being investigated. The results will be reported in the near future.

Acknowledgements

We thank the financial supports from the Korea Institute of Science and Technology (Grant No. 2E26130 & 2E26330) and from the Industrial Strategic Technology Development Program (Grant No. 10041589) funded by the Ministry of Trade, Industry, and Energy (MOTIE) of Korea. This work was also supported by the National Research Foundation of Korea Grant funded by the Korean Government (MSIP) (NRF-2011-C1AA001-0030538).

Electronic supplementary information (ESI) available: Details regarding development of ReaxFF, and additional results regarding preparation, lithiation and delithiation of SiO_x NWs.

References

- (1) U. Kasavajjula, C. S. Wang, A. J. Appleby, *J. Power Sources* 2007, **163**, 1003–1039.
- (2) M. N. Obrovac, L. Christensen, *Electrochim. Solid-State Lett.* 2004, **7**, A93–A96.
- (3) M. N. Obrovac, L. J. Krause, *J. Electrochem. Soc.* 2007, **154**, A103–A108.
- (4) X. H. Liu, L. Q. Zhang, L. Zhong, Y. Liu, H. Zheng, J. W. Wang, J.-H. Cho, S. A. Dayeh, S. T. Picraux, J. P. Sullivan, S. X. Mao, Z. Z. Ye, J. Y. Huang, *Nano Lett.* 2011, **11**, 2251–2258.
- (5) D. Larcher, S. Beattie, M. Morcrette, K. Edström, J. C. Jumas, J.-M. Tarascon, *J. Mater. Chem.* 2007, **17**, 3759–3772.
- (6) S. Zhou, X. Liu, D. Wang, *Nano Lett.* 2010, **10**, 860–863.
- (7) A. Magasinski, P. Dixon, B. Hertzberg, A. Kvít, J. Ayala, G. Yushin, *Nat. Mater.* 2010, **9**, 353–358.
- (8) C. K. Chan, H. Peng, G. Liu, K. McIlwrath, X. F. Zhang, R. A. Huggins, Y. Cui, *Nat. Nanotechnol.* 2008, **3**, 31–35.
- (9) L. F. Cui, R. Ruffo, C. K. Chan, H. Peng, Y. Cui, *Nano Lett.* 2009, **9**, 491–495.
- (10) H. Kim, M. Seo, M.-H. Park, J. Cho, *Angew. Chem., Int. Ed.* 2010, **49**, 2146–2149.
- (11) T. Song, J. Xia, J.-H. Lee, D. H. Lee, M.-S. Kwon, J.-M. Choi, J. Wu, S. K. Doo, H. Chang, W. I. Park, D. S. Zang, H. Kim, Y. Huang, K.-C. Hwang, J. A. Rogers, U. Paik, *Nano Lett.* 2010, **10**, 1710–1716.
- (12) B. Y. Yu, L. Gu, C. Zhu, S. Tsukimoto, P. A. van Aken, J. Maier, *Adv. Mater.* 2010, **22**, 2247–2250.
- (13) M.-H. Park, M.-G. Kim, J. Joo, K. Kim, J. Kim, S. Ahn, Y. Cui, J. Cho, *Nano Lett.* 2009, **9**, 3844–3847.

- (14) S.-H. Ng, J. Wang, D. Wexle, K. Konstantinov, Z.-P. Guo, H.-K. Liu, *Angew. Chem., Int. Ed.* **2006**, *45*, 6869-6899.
- (15) M. T. McDowell, S. W. Lee, C. Wang, Y. Cui, *Nano Energy* 2012, **1**, 401–410.
- (16) J. Luo, X. Zhao, J. Wu, H. D. Jang, H. H. Kung, J. Huang, *J. Phys. Chem. Lett.* 2012, **3**, 1824–1829.
- (17) T. Kim, S. Park, S. M. Oh, *J. Electrochem. Soc.* 2007, **154**, A1112-A1117.
- (18) K. Song, S. Yoo, K. Kang, H. Heo, Y.-M. Kang, M.-H. Jo, *J. Power Sources*. 2013. **229**, 229-233.
- (19) Y. Nagao, H. Sakaguchi, H. Honda, T. Fukunaga, T. Esaka, *J. Electrochem. Soc.* 2004, **151**, A1572-A1575.
- (20) W.-S. Chang, C.-M. Park, J.-H. Kim, Y.-U. Kim, G. Jeong, H.-J. Sohn, *Energy Environ. Sci.* 2012, **5**, 6895.
- (21) M. Miyachi, H. Yamamoto, H. Kawai, T. Ohta, M. Shirakata, *J. Electrochem. Soc.* 2005, **152**, A2089-A2091.
- (22) P. R. Abel, Y.-M. Lin, H. Celio, A. Heller, C. B. Mullins, *ACS Nano*. 2012, **6**, 2506-2516.
- (23) F. Iacona, C. Bongiorno, C. Spinella, S. Boninelli, F. Priolo, *Appl. Phys. Lett.* 2004, **95**, 3723.
- (24) Y. Q. Wang, R. Smirani, G. G. Ross, *J. Cryst. Growth* 2006, **294**, 486-489.
- (25) C. M. Park, W. Choi, W. Hwa, J.-H. Kim, G. Jeong, H.-J. Sohn. *J. Mater. Chem.* 2010, **20**, 4854-4860.
- (26) M. Mamiya, H. Takei, M. Kikuchi, C. Uyeda, *J. Cryst. Growth* 2001, **229**, 457-461.
- (27) M. Mamiya, M. Kikuchi, H. Takei, *J. Cryst. Growth* 2002, **237**, 1909-1914.
- (28) H. Wu, G. Chan, J. W. Choi, I. Ryu, Y. Yao, M. T. McDowell, S. W. Lee, A. Jackson, Y.

- Yang, L. Hu, Y. Cui, *Nat. Nanotech.* 2012, **7**, 309-314.
- (29) M. T. McDowell, S. W. Lee, I. Ryu, H. Wu, W. D. Nix, J. W. Choi, Y. Cui, *Nano Lett.* 2011, **11**, 4018-4025.
- (30) B. Hertzberg, A. Alexeev, G. Yushin, *J. Am. Chem. Soc.* 2010, **132**, 8548-8549.
- (31) J. Y. Huang, L. Zhong, C. M. Wang, J. P. Sullivan, W. Xu, L. Q. Zhang, S. X. Mao, N. S. Hudak, X. H. Liu, A. Subramanian, H. Fan, L. Qi, A. Kushima, J. Li, *Science* 2010, **330**, 1515-1520.
- (32) Z. Favors, W. Wang, H. H. Bay, A. George, M. Ozkan, C. S. Ozkan, *Sci. Rep.* 2014, **4**, 4605.
- (33) L. Tao, Z. Zai, K. Wang, H. Zhang, M. Xu, J. Shen, Y. Su, X. Qian, *J. Power Sources* 2012, **202**, 230-235.
- (34) C. Ban, B. B. Kappes, Q. Xu, C. Engtrakul, C. V. Ciobanu, A. C. Dillon, Y. Zhao, *Appl. Phys. Lett.* 2012, **100**, 243905.
- (35) A. M. Glass, K. Nassau, *J. Appl. Phys.* 1980, **51**, 3756-3761.
- (36) Y. Zhang, Y. Li, Z. Wang, K. Zhao, *Nano Lett.* 2014, **14**, 7161-7170.
- (37) C.-Y. Chou, G. S. Hwang, *Chem. Mater.* 2013, **25**, 3435-3440.
- (38) S. Perez-Beltran, G. E. Ramirez-Caballero, P. B. Balbuena, *J. Phys. Chem. C* 2015, **119**, 16424-16431.
- (39) A. C. T. van Duin, S. Dasgupta, F. Lorant, W. A. Goddard III, *J. Phys. Chem. A* 2001, **105**, 9396–9409.
- (40) A. C. T. van Duin, A. Strachan, S. Stewman, Q. Zhang, X. Xu, W. A. Goddard III, *J. Phys. Chem. A* 2003, **107**, 3803–3811.
- (41) H. Jung, M. Lee, B. C. Yeo, K.-R. Lee, S. S. Han, *J. Phys. Chem. C* 2015, **119**, 3447-3455.

- (42) A. C. T. van Duin, J. M. A. Baas, B. van der Graaf, *J. Chem. Soc. Faraday Trans.* 1994, **90**, 2881-2895.
- (43) A. Ostadhossein, S.-Y. Kim, E. D. Cubuk, Y. Qi, A. C. T. van Duin, *J. Phys. Chem. A* 2016, **120**, 2114-2127.
- (44) S. Plimpton, *J. Comput. Phys.* 1995, **117**, 1–19.
- (45) L. Verlet, *Phys. Rev.* 1967, **159**, 98-103.
- (46) W. G. Hoover, *Phys. Rev. A*. 1985, **31**, 1695-1697.
- (47) S. C. Jung, H.-J. Kim, J.-H. Kim, Y.-K. Han, *J. Phys. Chem. C* 2016, **120**, 886-892.
- (48) Q. Sun, B. Zhang, Z.-W. Fu, *Appl. Surf. Sci.* 2008, **254**, 3774–3779.
- (49) A. C. Ugural, S. K. Fenster, *Advanced Mechanics of Materials and Applied Elasticity (5th Edition)*; Pearson Education, Inc.: Boston, U.S.A., 2012.
- (50) W. H. Wang, *Prog. Mater. Sci.* 2012, **57**, 487–656.
- (51) Z. Zeng, N. Liu, Q. Zeng, Y. Ding, S. Qu, Y. Cui, W. L. Mao, *J. Power Sources* 2013, **242**, 732–735.
- (52) P. Vashishta, R. K. Kalia, A. Nakano, J. P. Rino, *J. Appl. Phys.* 2008, **103**, 083504.
- (53) S. C. Jung, Y. K. Han, *J. Phys. Chem. Lett.* 2013, **4**, 2681-2685.
- (54) S.-Y. Kim, A. Ostadhossein, A. C. T. van Duin, X. Xiao, H. Gao, Y. Qi, *Phys. Chem. Chem. Phys.* 2016, **18**, 3706-3715.
- (55) J.-L. Zang, Y.-P. Zhao, *Composites Part B* 2012, **43**, 76-82.

Figure Captions

Figure 1. ReaxFF-MD snapshots of the lithiation processes of SiO_x NWs (b-d). For comparison, the MD results for a pristine Si NW are also included (a). Here, the top, middle, and bottom figures represent the MD results at 0, 400, and 2,000 ps, respectively. The color codes for the atoms are as follows: yellow = Si, red = O, and pink = Li. The Li_xSi compositions and degrees of volume expansion are also shown in each figure.

Figure 2. (a) Volume changes and (b) Li concentration profiles of pristine Si and SiO_x NWs during lithiation, as obtained from the ReaxFF-MD simulations presented in Figure 1. (c) Plot of the volume change versus Li concentration. The black, gray, orange and red colors represent $\text{SiO}_{0.00}$ (pristine Si), $\text{SiO}_{0.14}$, $\text{SiO}_{0.29}$ and $\text{SiO}_{0.32}$ NWs, respectively.

Figure 3. RDF $g(r)$ analyses for (a-c) Si-Si, (d-f) Si-O, (g-i) Si-Li, and (j-l) O-Li pairs in the pristine and SiO_x NWs during lithiation, as obtained from the ReaxFF-MD simulations presented in Figure 1. The color codes are as follows: black = pristine Si, green = $\text{SiO}_{0.14}$, red = $\text{SiO}_{0.29}$, and blue = $\text{SiO}_{0.32}$.

Figure 4. (a) A schematic figure showing the formation of interfaces in a SiO_x NW during the lithiation process, where the black interface indicates that between *c*-Si and *a*- SiO_2 phases in the initial SiO_x NW and the blue and green interfaces indicate those between the *a*- Li_xSiO_2

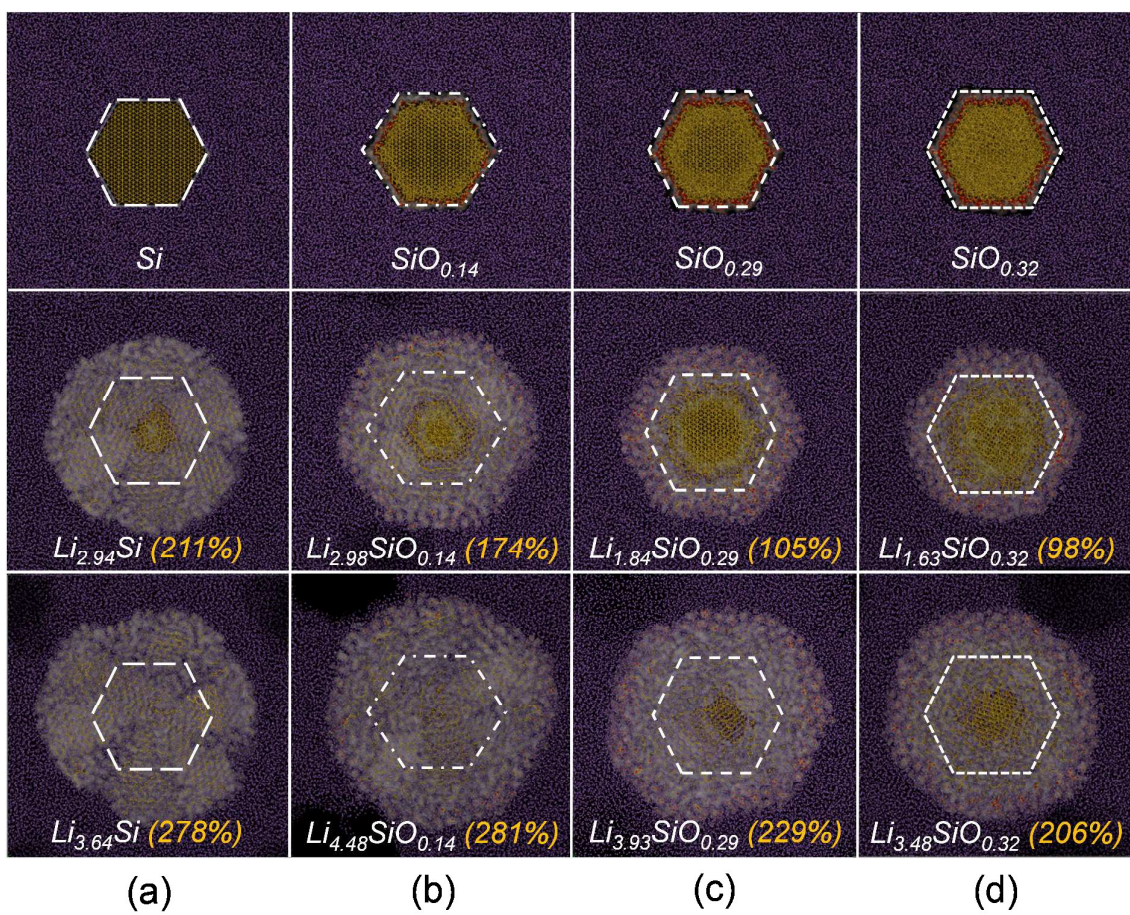
and $a\text{-Li}_x\text{Si}$ phases and between the $a\text{-Li}_x\text{Si}$ and $c\text{-Si}$ phases, respectively. (b-d) Concentration profiles.

Figure 5. Formation of Li_2O and Li_4SiO_4 compounds in the $\text{SiO}_{0.14}$ NW during lithiation. In (a), the core region is removed to focus on lithiation behaviors in the oxide layer.

Figure 6. Residual stress distributions of the (a) pristine Si and (b) SiO_x NWs during lithiation. Here, positive (+) and negative (-) values correspond to tensile and compressive stresses, respectively. Red bars in each figures indicate schematic structures of the NWs at 500 ps.

Figure 7. Comparison of the lithiation mechanisms for (a-e) pristine Si and (f-j) $\text{SiO}_{0.14}$ NWs. (k-m) top views showing the lithiation mechanism in the $\text{SiO}_{0.14}$ NW, where three processes of Li atoms, such as formation of Li_2O (purple Li atom) and Li_4SiO_4 (green Li atom) in the silicon oxide layer and diffusion (black Li atom) into the $c\text{-Si}$ region after passing through the SiO_2 layer without such formation of Li_2O and Li_4SiO_4 compounds, are observed. Here, most Li atoms are removed for clarity.

Figure 8. Dissociation and recombination of Li_4SiO_4 during lithiation. The color codes for the atoms are as follows: yellow = Si, red = O, and purple/blue/green = Li.

**Figure 1**

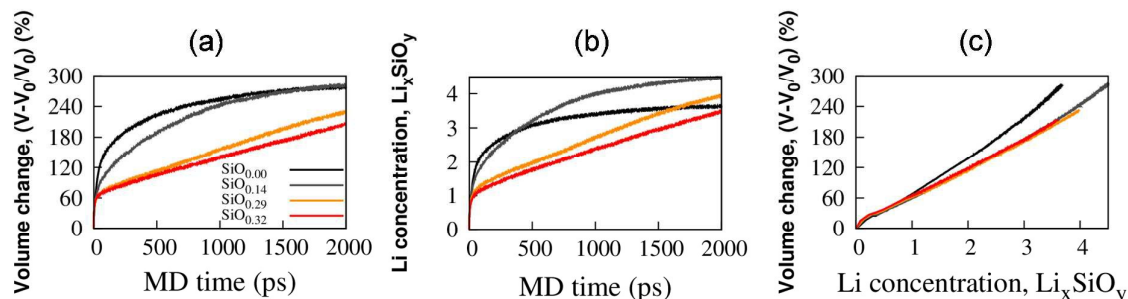
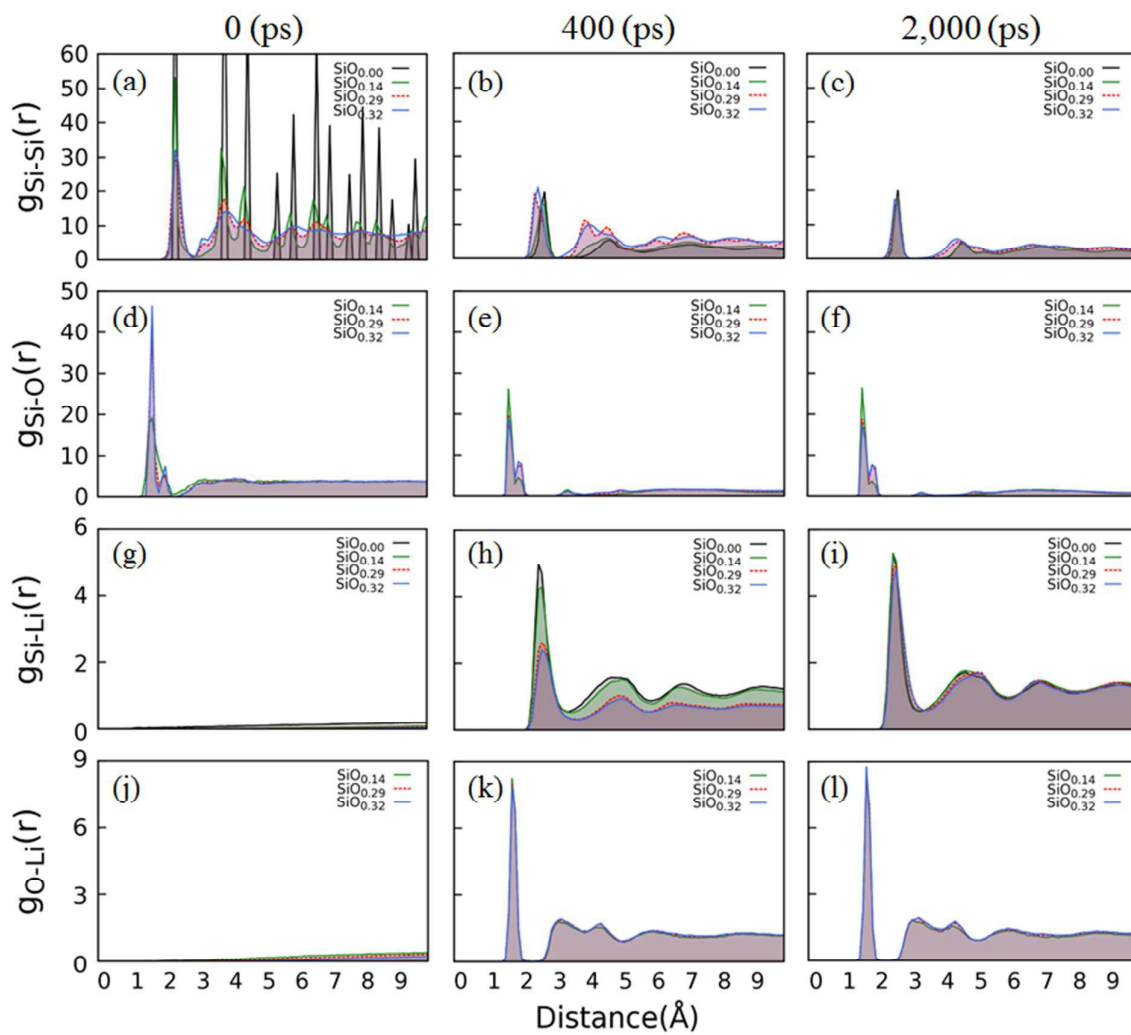
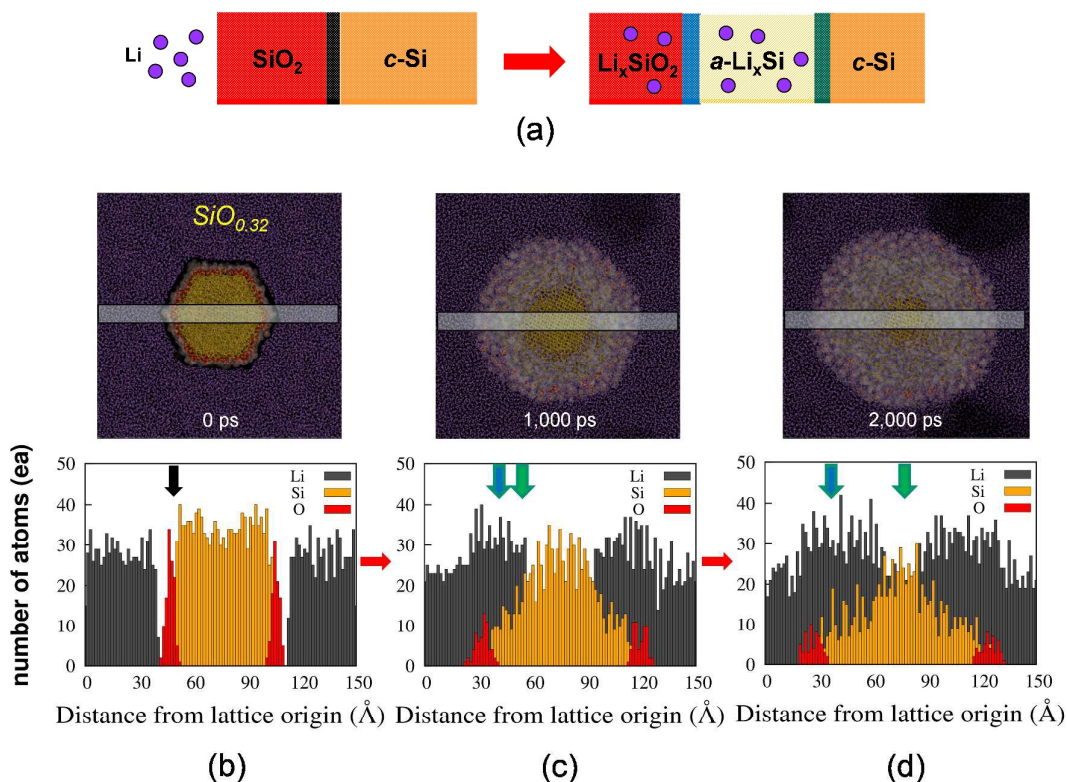


Figure 2

**Figure 3**

**Figure 4**

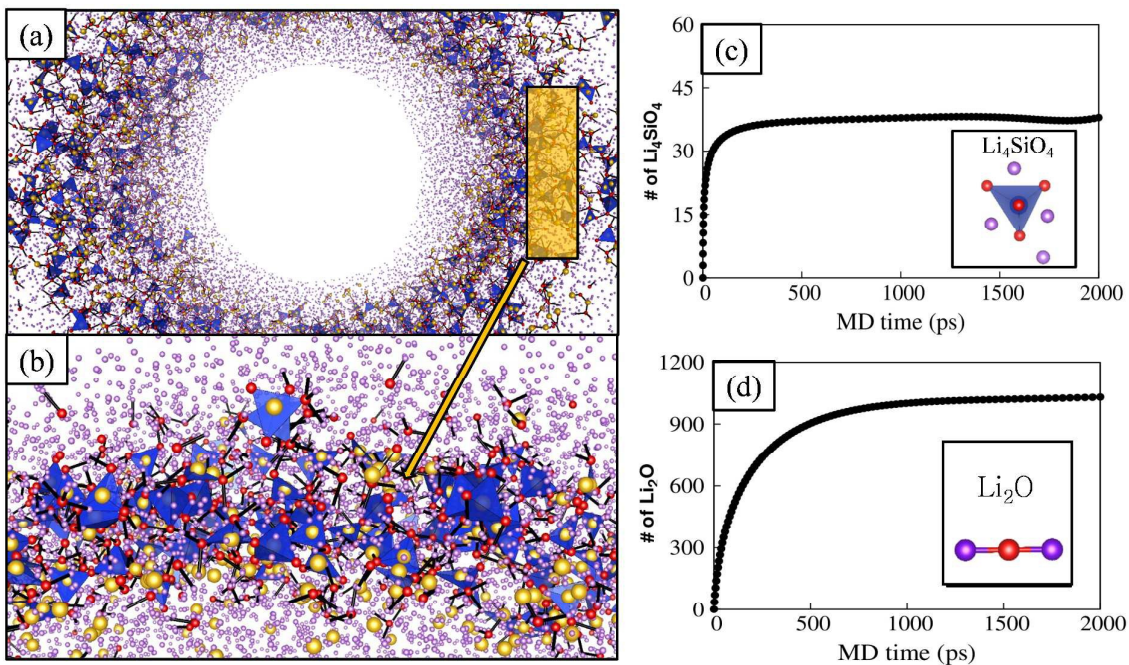


Figure 5

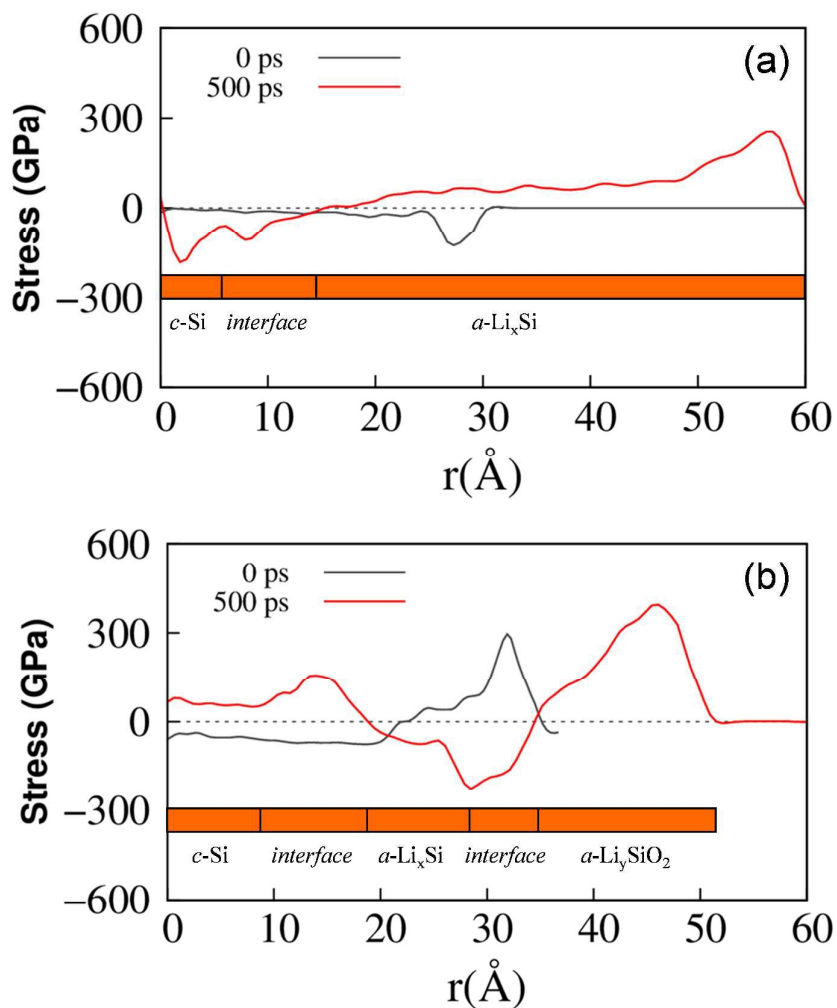


Figure 6

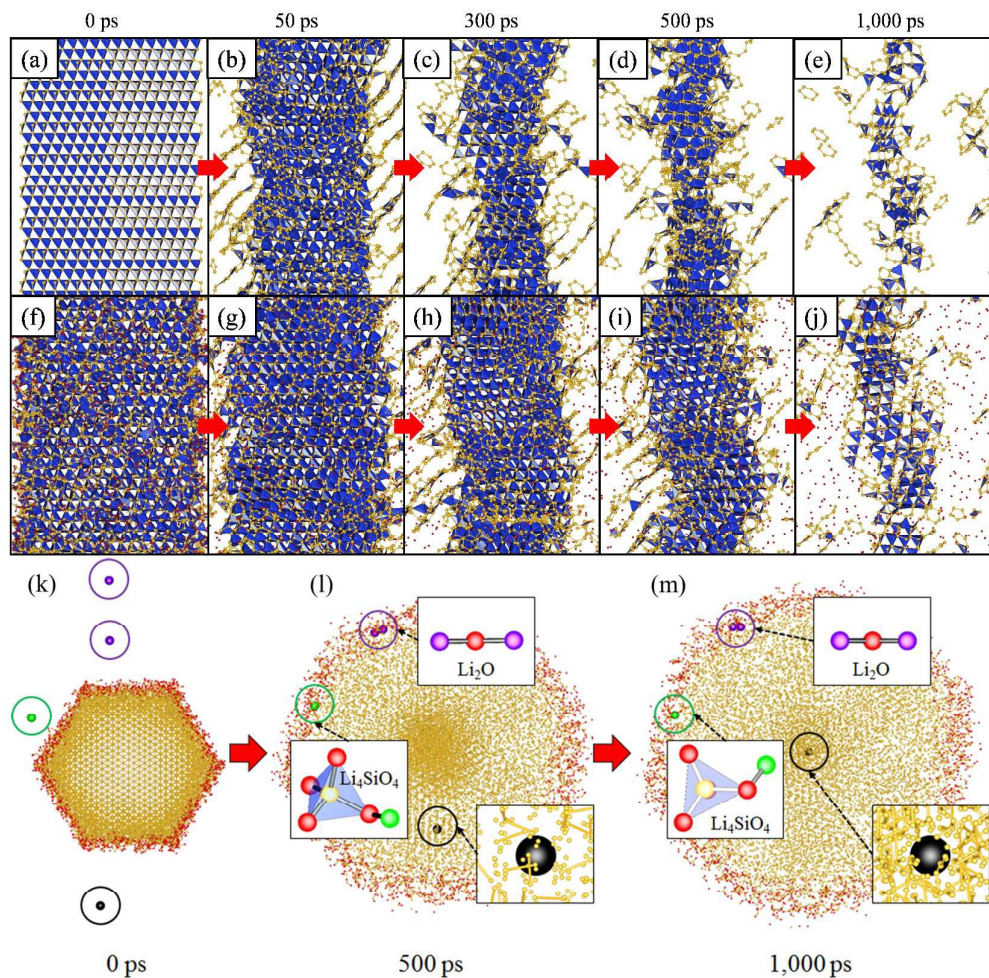


Figure 7

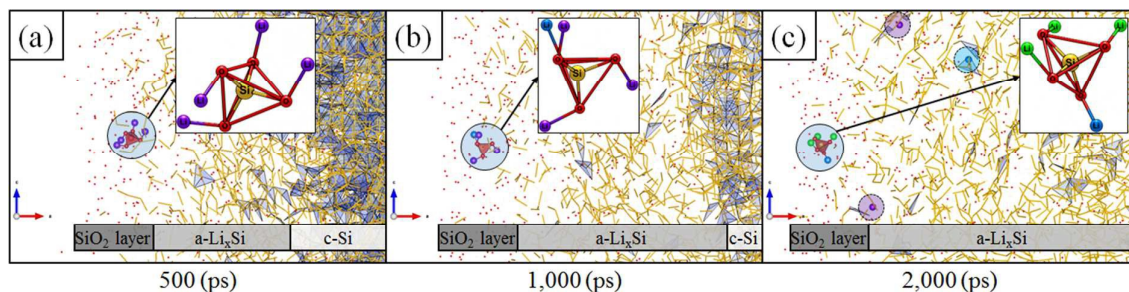
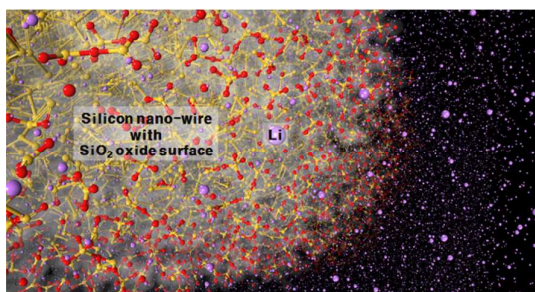


Figure 8

Graphical Abstract



The atomistic lithiation mechanism of silicon oxides (SiO_x) is clarified using the ReaxFF reactive molecular dynamics simulation.